Astron. Astrophys. 306, 219–231 (1996)

ASTRONOMY AND ASTROPHYSICS

Nonthermal ionization and excitation in Type IIb supernova 1993J

Victor P. Utrobin[1,2]

[1] Institute of Theoretical and Experimental Physics, B. Cheremushkinskaya St. 25, 117259 Moscow, Russia
[2] Max-Planck-Institut für Astrophysik, Karl-Schwarzschild-Str. 1, D-85740 Garching, Germany

Received 2 February 1995 / Accepted 20 May 1995

Abstract. A non-LTE study of Type IIb supernova 1993J in the galaxy M 81 accounting for nonthermal ionization and line blocking effects is carried out. Hydrodynamical models and theoretical spectra clearly show that nonthermal ionization and excitation dominate after the second maximum, at day ~ 30, and play a decisive role in reproducing both a smooth tail of the light curve and an emergence of helium lines in the spectrum similar to those observed. Based on our model of supernova 1993J, we predict that the light curves of Type Ib supernovae should be subject to nonthermal ionization and excitation at earlier times than even that of supernova 1993J.

To fit the bolometric and visual light curves of supernova 1993J, an outer layer of $\sim 1\ M_\odot$ has to be helium-rich hydrogen shell with a hydrogen mass fraction of ~ 0.1. In this shell there is no nearly pure helium mantle as contrasted to most of the evolutionary models at the time of explosion. The fact that such a distribution of hydrogen results in a characteristic maximum of hydrogen number density at velocity of ~ 8600 km s^{-1} in the expelled envelope is well consistent with late time observations of Hα emission at epochs of $0.5-1$ year after the explosion. An emergence of helium lines between day 24 and day 30 illustrated by the evolution of calculated profile of the He I line λ6678Å completely fits the spectral observations of supernova 1993J.

The bolometric and visual light curves and the spectral evolution of helium lines are consistent with a mass of the ejected envelope of $\sim 2.4\ M_\odot$ including a hydrogen mass of $\sim 0.12\ M_\odot$, an explosion energy of $\sim\ 1.6 \cdot 10^{51}$ ergs, and a mass of radioactive ^{56}Ni of $\sim 0.078\ M_\odot$. It is found that the bulk of the radioactive material should be confined to layers of the ejected envelope expanding with velocities less than ~ 3800 km s^{-1}.

In our model, the outburst of supernova 1993J is interpreted as the explosion of a $\sim 4\ M_\odot$ red supergiant undergoing core collapse and leaving a neutron star in a binary system. The progenitor is supposed to have a helium core mass of $\sim 3\ M_\odot$ corresponding to a $\sim 13\ M_\odot$ main-sequence star. Supernova 1993J adds evidence to the scenario that Type Ib supernovae originate from moderately massive stars on the main sequence which have lost their hydrogen envelopes in interacting binary systems. It is shown that there are strong arguments in favor of a fundamental similarity between the explosions of Type IIb, Ib, and II-P supernovae.

Key words: supernovae: SN 1993J – supernovae: general

1. Introduction

Soon after its discovery supernova (SN) 1993J in the galaxy M 81 (NGC 3031) was classified as a Type II supernova (SN II). Further extensive photometric observations revealed an unprecedented visual light curve with two distinct maxima. It was clear that SN 1993J was different from the classical variety of Type II supernovae (SNe II). Moreover, optical spectra of SN 1993J showed the onset of a remarkable transformation from the characteristics of SNe II to those of SNe Ib (Filippenko et al. 1993; Swartz et al. 1993). The Hα emission line prominent at early times became gradually weaker and was progressively superimposed by the He I line λ6678Å after the second peak as helium absorption and emission features developed.

A good agreement between hydrodynamical models and the available observational data of this event led Höflich et al. (1993b), Podsiadlowski et al. (1993), Wheeler et al. (1993), Bartunov et al. (1994), Shigeyama et al. (1994), Utrobin (1994a), and Woosley et al. (1994) to conclude that the low hydrogen mass of the expelled envelope was a distinguishing feature of SN 1993J. Such a hydrogen mass implies that very likely the progenitor of SN 1993J has lost most of its hydrogen-rich envelope prior to the explosion. All but Höflich et al. (1993b) reached the conclusion that SN 1993J was produced by a star with an initial main-sequence mass in the range of $\sim 12-16\ M_\odot$ which lost most of its hydrogen-rich envelope during a close binary evolutional phase.

A comprehensive review of both observational data and theoretical studies on SN 1993J for the first three months of its outburst was given by Wheeler & Filippenko (1994).

An emergence of strong helium absorption and emission features in the optical spectra of SN 1993J as well as SNe Ib may

Send offprint requests to: V.P. Utrobin

be attributed to nonthermal excitation. Harkness et al. (1987), analyzing synthetic spectra, were the first to identify the strong absorption troughs in the optical spectra of SNe Ib with helium lines. Lucy (1991) convincingly showed that these helium lines were solely due to nonthermal excitation induced by nonthermal electrons which are created by Compton scatterings of γ-rays emitted in radioactive ^{56}Co decay. Using spectral synthesis techniques Swartz et al. (1993) computed atmosphere models of SN 1993J at a phase of $\sim$ 40 days after shock break out when the strong helium lines definitely appeared in the optical and infrared. Baron et al. (1994) compared non-LTE spectral synthesis models with the ultraviolet and optical spectra of SN 1993J at a phase of $\sim$ 17 days and required a significant amount of nonthermal ionization. These atmosphere models fitted the observed spectra well and were consistent in general terms with the hydrodynamical models discussed above.

The present work is a continuation of the previous paper on hydrodynamical study of SN 1993J (Utrobin 1994a). Here we invoke nonthermal ionization and excitation in order to reproduce the observed light curves and to throw light upon the physical nature of their smoothness. We also compute theoretical profiles of helium lines in the frame of our favored hydrodynamical model and investigate the emergence of strong helium lines in the optical spectrum. Input physics and computational method are briefly described in Sect. 2. In Sect. 3 the initial model and hydrodynamics of the explosion are presented. The nature of the bolometric light curve is discussed and the influence of nonthermal ionization and line blocking effects on the bolometric and visual light curves is studied in Sect. 4. The non-LTE formation of helium lines and their emergence in the optical follow in Sect. 5. In Sect. 6 the obtained results and the physical relation between SNe Ib, SNe IIb, and SNe II-P are discussed, and our conclusions are drawn. Note that we have already presented preliminary results of this study (Utrobin 1994b).

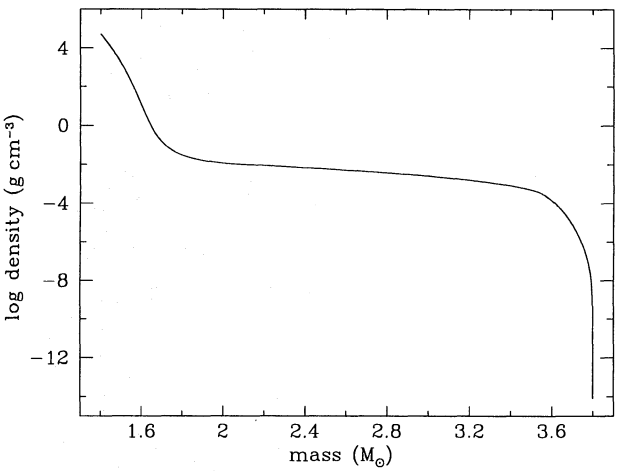

Fig. 1. Density distribution with respect to interior mass for the presupernova model NTLB

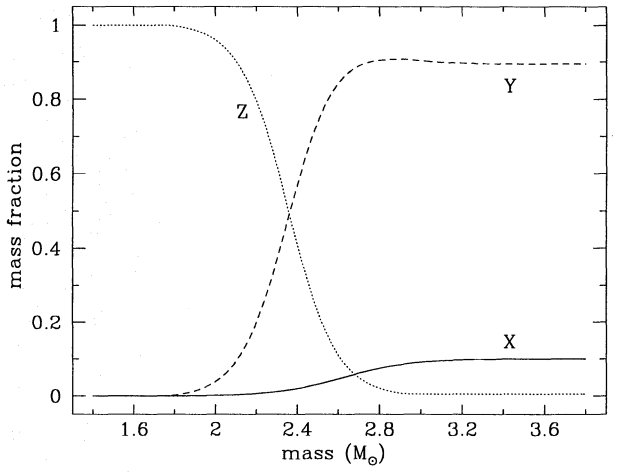

Fig. 2. The mass fraction of hydrogen (X), helium (Y), and heavy elements (Z) in the ejected envelope for model NTLB. The total mass of hydrogen, helium, and heavy elements in the ejecta is 0.12 $M_\odot$, 1.32 $M_\odot$, and 0.96 $M_\odot$, respectively. The central core of 1.4 $M_\odot$ is omitted

2. Input physics and computational method

The supernova hydrodynamical models discussed below are based on a numerical integration of the equations of radiation hydrodynamics for a gas that moves with spherical symmetry in its own gravitational field.

2.1. Basic approximations

The equations of radiation hydrodynamics are treated in the approximation of equilibrium radiative diffusion. The radiative diffusion is computed in accordance with a flux-limited diffusion theory of Levermore & Pomraning (1981). As initial conditions for these equations we employ polytropic-like stellar models in hydrostatic equilibrium. An implicit finite-difference scheme is used to integrate the equations of radiation hydrodynamics. To calculate shock waves, we apply the pseudo-viscosity method. In our computed models the star is subdivided into 200 mass layers.

The following elements are included in the non-LTE gas equation of state: H, He, C, N, O, Ne, Na, Mg, Si, S, Ar, Ca, and Fe. All but H are treated with the 3 ionization stages. Atomic weights and ionization potentials are from Allen (1973). Radiative and dielectronic recombination rate coefficients are all taken from Shull & Van Steenberg (1982), except for H I and He I. Recombinations to the ground state of these two ions lead to immediate reionization, so they are omitted and radiative recombination rate coefficients for Case B are used (Osterbrock 1989). The dielectronic recombination rate coefficient for He I is from Aldrovandi & Péquignot (1973).

2.2. Nonthermal ionization and excitation

At each time step, the non-LTE ionization balance of the above mixture is found involving the relevant rates of nonthermal ion-

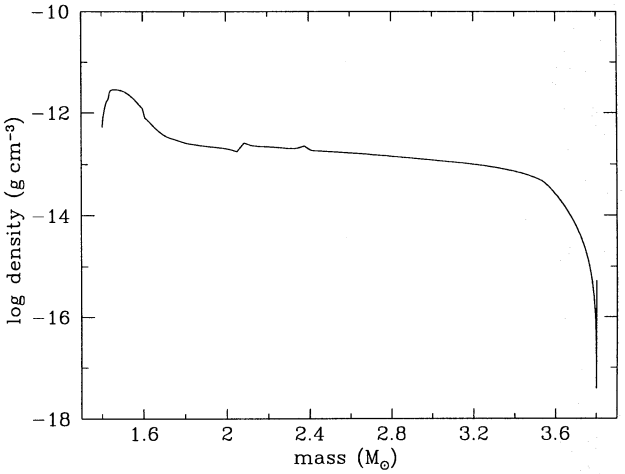

Fig. 3. Density profile with respect to interior mass at day 20 for model NTLB

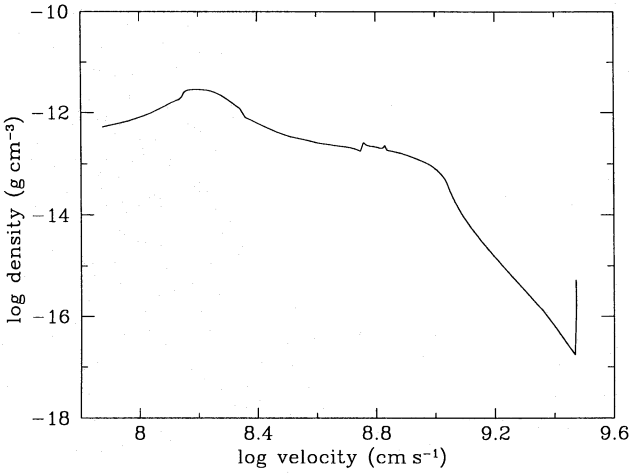

Fig. 5. Density profile with respect to the expansion velocity at day 20 for model NTLB

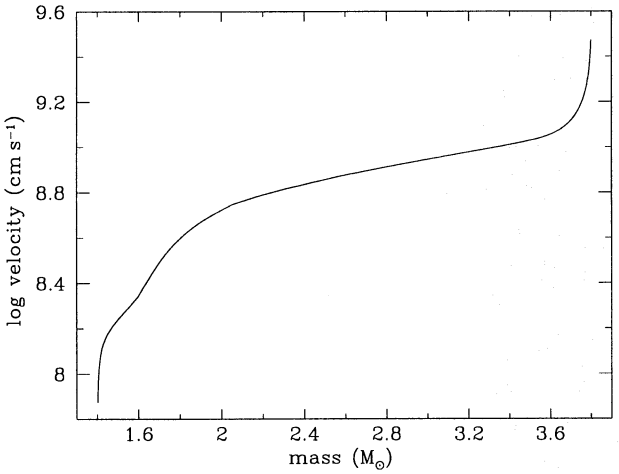

Fig. 4. Velocity profile with respect to interior mass at day 20 for model NTLB

ization. Nonthermal ionizations and excitations discussed here are due to impacts by nonthermal electrons which are created by Compton scatterings of the γ-rays, emitted in radioactive ^{56}Ni and ^{56}Co decay, in a free and bound electrons, and then by the subsequent degradation of Compton electrons in energy.

The transport of γ-rays is treated in an approximation similar to that of Sutherland & Wheeler (1984) with an effective γ-ray absorption opacity of 0.03 cm^2 g^{-1} for an electron to nucleon ratio of 0.5. The latter was inferred by Colgate et al. (1980) from Monte Carlo calculations. Note that Ambwani & Sutherland (1988) compared the rate at which energy is deposited by scattering and absorption of γ-rays in supernova ejecta, taken from Monte Carlo studies, to that calculated with their absorption model and found excellent agreement between the two methods.

The Compton electrons, resulting from Compton scatterings of γ-rays in the free and bound electrons, are assumed to lose their energy locally. They deposit their energy by heating free electrons, ionizing and exciting atoms and ions. So the decay energy of radioactive ^{56}Ni and ^{56}Co is reprocessed into heating, excitation, and ionization. Kozma & Fransson (1992) have calculated the γ-ray deposition in supernovae by solving the Spencer-Fano equation and have given convenient analytical expressions of ionization, excitation, and heating rates for different chemical compositions. We apply their results of the hydrogen envelope (solar abundances), the helium-carbon zone, and the oxygen-silicon-sulphur zone for computing the rates of nonthermal ionization.

2.3. Opacity and line blocking effects

After finding the non-LTE ionization balance, the Rosseland mean opacity is evaluated in the hydrogenic approximation, allowing for Thomson scattering from free electrons, free-free, and bound-free photoionization from ground state of all ions listed above. A contribution of the negative hydrogen ion to the opacity is calculated according to Doughty & Fraser (1966).

As pointed out by Karp et al. (1977), in rapidly expanding envelopes the opacity can be significantly increased due to line blocking effects. This influence of lines on the opacity is particularly important for the envelope layers composed of heavy elements. In order to account adequately for the line blocking contribution to the opacity of these layers, we use the enhancement factor tables for the carbon-oxygen-rich composition mixtures calculated by Höflich et al. (1993a). The corresponding Rosseland mean expansion opacity is directly determined by the enhancement factor and the Thomson opacity.

3. Hydrodynamical model

Of the various hydrodynamical models calculated to discriminate the proper model parameters, the model NTLB with a mass of the ejected envelope of 2.4 $M_\odot$, an explosion energy

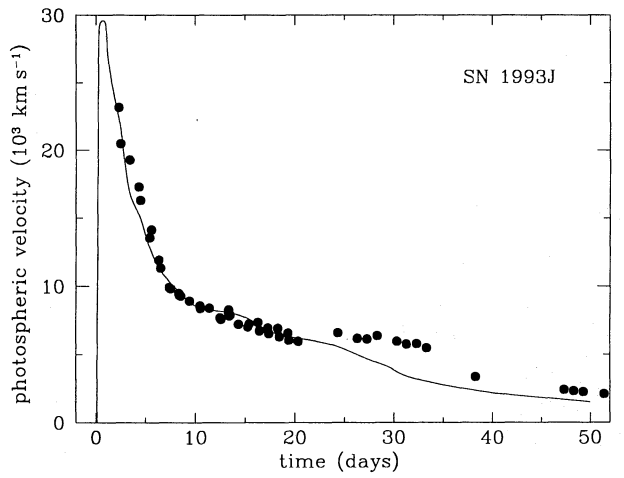

Fig. 6. Time dependence of the velocity at the photosphere for model NTLB. Solid circles give the photospheric velocity derived from the observational data for SN 1993J (Lewis et al. 1994) on the assumption of a homologous expansion

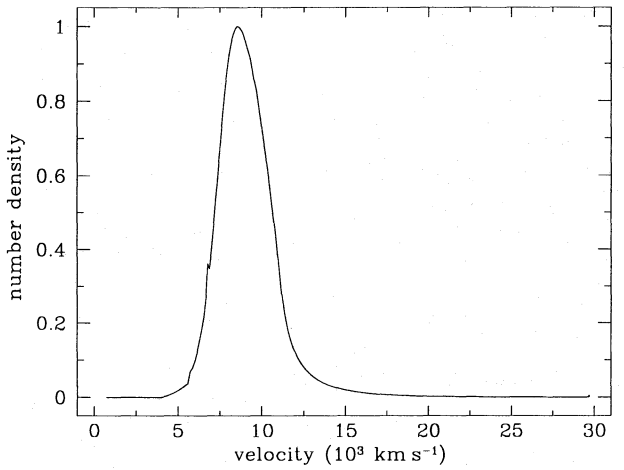

Fig. 7. Hydrogen number density profile normalized to a maximum number density of $6.6 \cdot 10^9$ cm^{-3} at a velocity of ~ 8600 km s^{-1} with respect to the expansion velocity at day 20 for model NTLB

of $1.6 \cdot 10^{51}$ ergs, and a mass of radioactive ^{56}Ni of 0.078 $M_\odot$ is selected since it reproduces the bolometric and visual light curves of SN 1993J very well. This model takes account of both nonthermal ionization and line blocking effects. Note that in this paper the time of observations is reckoned from 1993 March 28.1 UT.

3.1. Initial model and chemical composition

To investigate the dependence of the bolometric light curve on the density profile, we have constructed a hydrostatic model consisting of a central white dwarf like core and an outer envelope with a polytropic structure of index n_S. In the hydrodynamical model presented below, the central core is removed from the computational mass grid and taken into account by an inner boundary condition at fixed radius and interior mass. The central core is merged with the outer envelope by an intermediate shell. Its density profile is characterized by some polytropic index n_C and smoothly joins with that of the outer envelope. The advantage of such a hydrostatic model is that shells of various mass and density profile can be explored, while the central core and the outer envelope are fixed.

To fit the bolometric and visual light curves of SN 1993J, a set of hydrostatic models with different chemical compositions has been explored. The best fit has been obtained with model NTLB. The presupernova model has a photospheric radius of ~ 434 $R_\odot$. It is characterized by the density profile shown in Fig. 1 and the chemical composition in Fig. 2. Its central core is similar to a white dwarf having a mass of 1.4 $M_\odot$ and a radius of 10^{-2} $R_\odot$. Its outer envelope has a polytropic index $n_S = 4.95$. In this model the 1.4 $M_\odot$ central core is assumed to collapse to a neutron star of 1.26 $M_\odot$ while the rest of the envelope of 2.4 $M_\odot$ is ejected by the explosion. The ejecta of model NTLB consist of a 0.96 $M_\odot$ inner shell of heavy elements with an oxygen mass fraction of ~ 0.77 and an ~ 1 $M_\odot$ outer layer of helium-rich material with a hydrogen mass fraction of ~ 0.1.

3.2. Evolution of density structure

The explosion of the star is assumed to be triggered by an instantaneous energy release near the edge of the central core at epoch zero. This instantaneous release of energy leads to the formation of a strong shock wave which propagates towards the stellar surface. In moving out of the center, the shock wave heats matter and accelerates it to velocities increasing outward. As the shock wave reaches the outermost layers, they are accelerated due to a sharp decline in density (Fig. 1). The density and velocity distributions with respect to interior mass at day 20 clearly show that only a small portion of the star undergoes such an acceleration and acquires a high velocity (Figs. 3 and 4). These outer layers are characterized by an effective index $q = -\partial \lg \rho / \partial \lg v$ of ~ 7 as seen from the density distribution with respect to the expansion velocity at day 20 (Fig. 5).

3.3. Comparison with observations

In addition to the bolometric light curve for SN 1993J, Lewis et al. (1994) and Richmond et al. (1994) have provided the time dependence of the photospheric radius. On the assumption of homologous expansion valid for the layers at the photosphere, we consider the velocity obtained from the photospheric radius divided by the corresponding time after the explosion as a measure of the photospheric velocity. The calculated photospheric velocity is in good agreement with the observations of SN 1993J up to day 20 (Fig. 6). But between day 20 and day 40 it departs from the observations. The good fit of the calculated velocity at the photosphere during the first 20 days (Fig. 6) suggests that the radial velocity profile in the hydrodynamical model is relevant to that in the ejected envelope of SN 1993J.

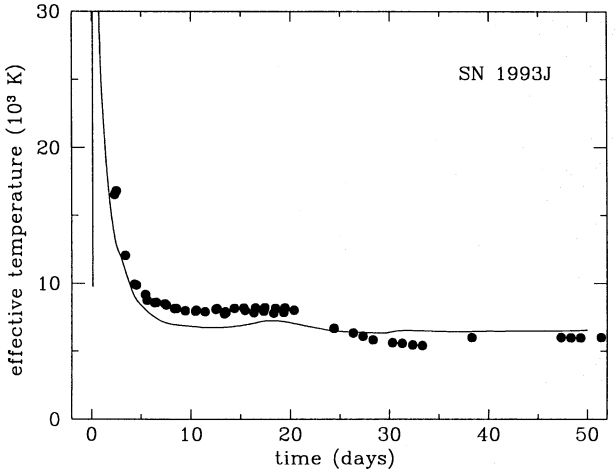

Fig. 8. Time dependence of the effective temperature. The solid line represents model NTLB and solid circles give the observational data for SN 1993J obtained by Lewis et al. (1994)

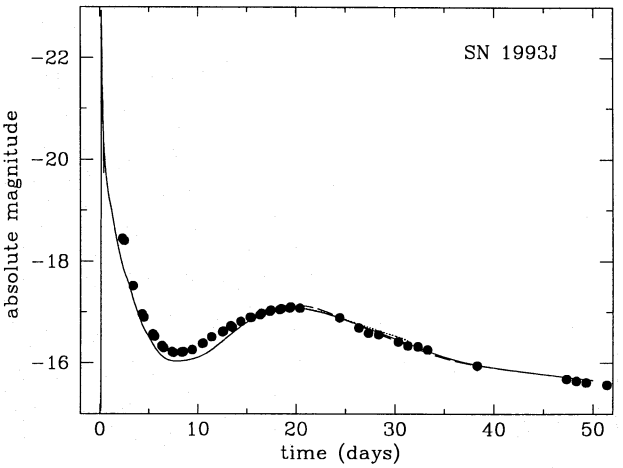

Fig. 9. Comparison of the calculated light curve of models NTLB (solid line), NT (dash line), and LB (dotted line) with the bolometric data for SN 1993J obtained by Lewis et al. (1994). Model NT includes nonthermal ionization but not line blocking effects. On the contrary, model LB includes line blocking effects but not nonthermal ionization. All calculated curves are practically indistinguishable

The late time spectral observations of SN 1993J between 0.5 – 1 year after the explosion have revealed a specific profile of Hα emission. It implies that ionized hydrogen is distributed over a shell. Its maximum density of ionized hydrogen corresponds to 8900-9300 km s^{-1}, while the inner and outer edges have velocities of $\sim$ 7500 km s^{-1} and $\sim$ 11400 km s^{-1} respectively (Patat et al. 1994). The calculated distribution of hydrogen number density as a function of the expansion velocity at day 20 is shown in Fig. 7. It results from the chemical composition (Fig. 2) and the density and velocity distributions against interior mass (Figs. 3 and 4) and has a characteristic maximum at a velocity of $\sim$ 8600 km s^{-1} in the expelled envelope. It is clear that the calculated distribution of hydrogen is well consistent with the late time observations of Hα emission. The fact that the velocity distribution of hydrogen number density which is extracted from a fit of the observed bolometric and visual light curves is in a good agreement with the spectral observations of Hα emission is of great importance.

4. Light curves

Observations of SN 1993J at all wave bands have resulted in the bolometric light curve, the effective temperature and the photospheric radius as a function of time (Lewis et al. 1994; Richmond et al. 1994). In order to compare the calculated light curves with the observed ones, we take a distance modulus to the M 81 of $27\overset{m}{.}8$ and accept a total extinction towards M 81 of E(B-V) = $0\overset{m}{.}03$ (Freedman et al. 1994).

The outburst of SN 1993J under study has four stages: a shock break out, an epoch of intensive cooling and recombination in the envelope, a stage of the radioactive ^{56}Ni and ^{56}Co decay dominant in powering the luminosity with thermal ionization and excitation, and a stage of nonthermal ionization and excitation.

4.1. Stage of shock break out

In the first stage the shock wave reaches the stellar surface in 0.124 days after the core collapse and heats the external layers, so that the effective temperature jumps to $1.3 \cdot 10^5$ K (Fig. 8) and the bolometric luminosity rises accordingly (Fig. 9). The star then begins to expand, its outside layers cool very rapidly, and the luminosity decreases. A narrow peak of luminosity results. Most of the radiation is emitted in an ultraviolet flash. The peak has a width of $\sim$ 0.09 days and reaches a bolometric magnitude of -22.93 at maximum (Fig. 9). Note that the energy radiated during the first day adds up to $5 \cdot 10^{48}$ ergs.

4.2. Stage of intensive cooling and recombination

The second stage lasts from the time shortly after the shock wave arrives at the surface till day $\sim$ 7 and involves intensive cooling and recombination of outer layers due to the envelope expansion (Figs. 10 and 11). Both the effective temperature and the luminosity falls rapidly (Figs. 8 and 9). The internal energy of the envelope drops from $\sim 9.7 \cdot 10^{49}$ ergs to $\sim 1.9 \cdot 10^{48}$ ergs. From an inspection of the distribution of ionized hydrogen fraction and the interior luminosity distribution against mass it is evident that the luminosity of star at this phase is provided by radiative diffusion from the outside envelope layers of $\sim 0.4\ M_\odot$ where internal energy has been deposited by the shock wave (Figs. 10 and 12).

During this phase the first bolometric peak of high luminosity is converted by the large bolometric correction into a smaller one in the visual band (Fig. 13). Just after the bolometric luminosity reaches its maximum, the effective temperature drops so fast that the reduction of the bolometric correction dominates the decreasing bolometric luminosity and, in spite of it, results in

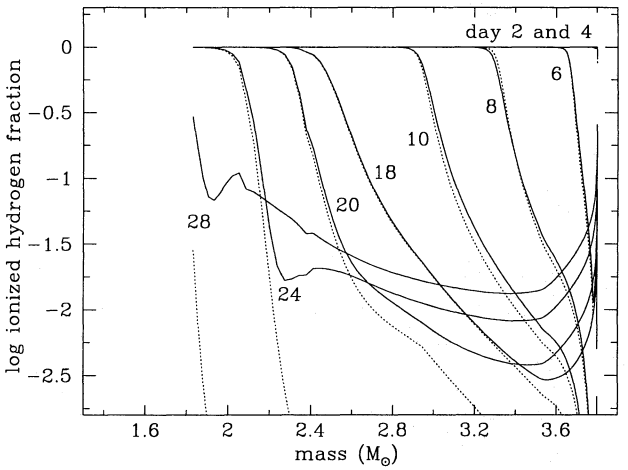

Fig. 10. Evolution of the fraction of ionized hydrogen as a function of mass for model NTLB (solid line) and LB (dotted line). Profiles are plotted at the indicated elapsed times

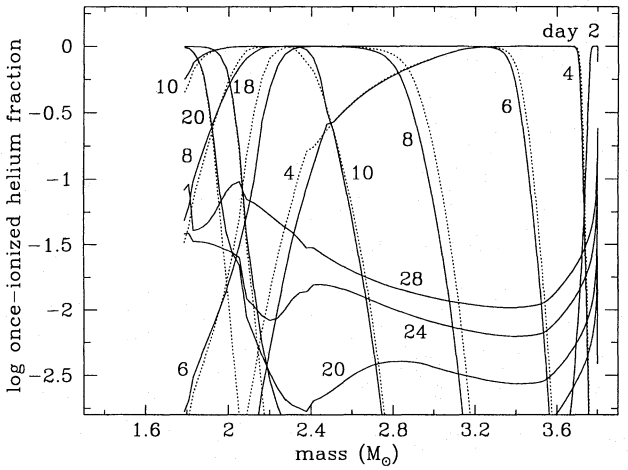

Fig. 11. Evolution of the fraction of once-ionized helium as a function of mass for models NTLB (solid line) and LB (dotted line). Profiles are plotted at the indicated elapsed times

a rise of the visual luminosity until day $\sim$ 2. Beginning around day 2 the visual light curve follows the bolometric one in shape and eventually forms two distinct maxima (Fig. 13 and 9).

4.3. Stage of radioactive ^{56}Ni and ^{56}Co decay

The third stage begins at the time of luminosity minimum at day $\sim$ 7. By this time the radiative diffusion wave carrying outward energy deposited by radioactive ^{56}Ni and ^{56}Co decay in the internal layers reaches the outer edge of the envelope (Fig. 12). As a consequence, the effective temperature and the luminosity decrease no longer (Figs. 8 and 9). It should be emphasized that from here on ^{56}Ni and ^{56}Co radioactive decays become entirely dominant in powering the supernova luminosity.

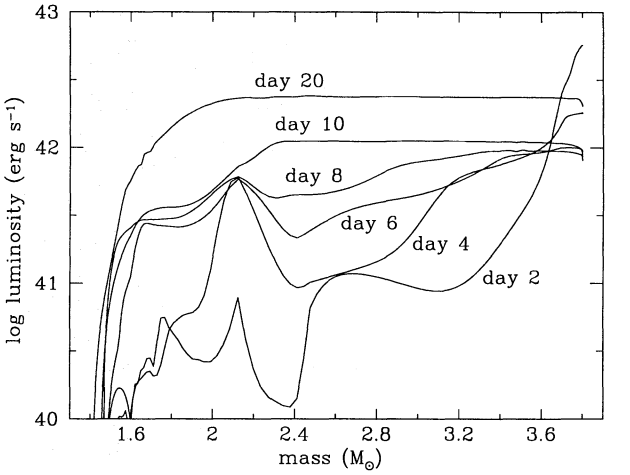

Fig. 12. Evolution of the interior luminosity as a function of mass for model NTLB. Luminosity profiles are plotted at the indicated elapsed times

Increasing the radiative diffusion of energy results in brightening the supernova (Figs. 12 and 9). The rate at which energy is deposited by radioactive ^{56}Ni and ^{56}Co decay in the inner layers is high enough to produce a rise of the luminosity to the second peak from day $\sim$ 7 to day $\sim$ 20 (Fig. 9), the effective temperature being virtually constant and $\sim$ 7000 K (Fig. 8). At this stage the effective temperature depends on the hydrogen to helium ratio in the outside envelope layers of $\sim$ 1.2 $M_\odot$. Then the light curve begins to decline at first rather modestly but later nearly as rapidly as the radioactive ^{56}Co decay does forming the second peak (Fig. 9). The radiative diffusion gradually reduces the internal energy of the expanding matter, and, for example, by day $\sim$ 40 it is merely of $\sim$ 3 $\cdot$ 10^{47} ergs.

The hydrogen recombination front moves inward in mass, as during the previous stage, while the radiative diffusion of energy propagates outward (Figs. 10 and 12). Note that by the time of the second peak the bulk of hydrogen and helium ions has recombined, the fraction of ionized hydrogen and once-ionized helium being less than $\sim$ 0.01 (Figs. 2, 10, and 11).

4.4. Stage of nonthermal ionization and excitation

To clarify the role of nonthermal ionization and excitation, and of line blocking effects for the formation of the light curve and to determine the beginning of a stage of dominant nonthermal processes, two additional models NT and LB have been computed. Model NT includes nonthermal ionization but not line blocking effects. Both the calculated bolometric and visual light curves of models NTLB and NT are practically indistinguishable (Figs. 9 and 13). Hence, the calculated light curves are insensitive to line blocking effects.

On the contrary, model LB includes line blocking effects but not nonthermal ionization. The calculated bolometric light curves of models NTLB and LB are also practically indistinguishable, but the visual ones differ drastically (Figs. 9 and 13).

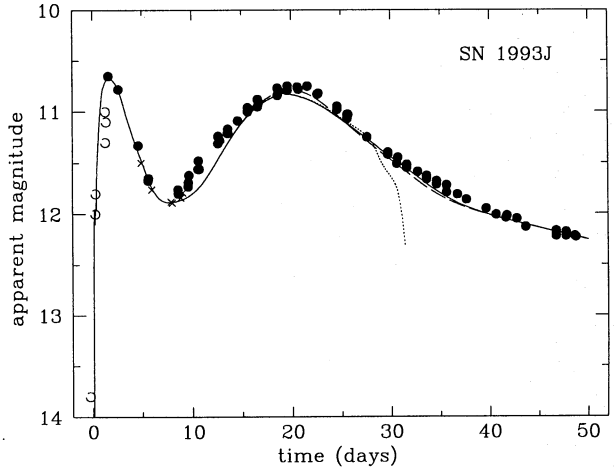

Fig. 13. Comparison of the calculated visual light curve of models NTLB (solid line), NT (dash line), and LB (dotted line) with the observational data of SN 1993J for the first 50 days. Open circles are the visual and unfiltered CCD observations of Neely (1993), Garcia (1993), Rodriguez (1993), and Pujol (1993). Crosses are the V observations of Kato (1993) and solid circles are those of Richmond et al. (1994)

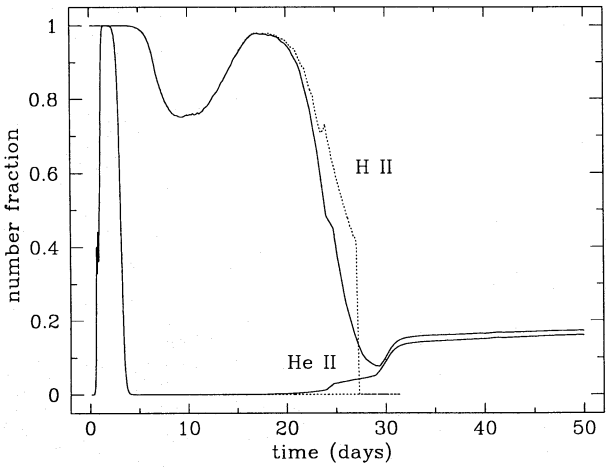

Fig. 14. Time dependence of the fraction of ionized hydrogen and once-ionized helium at the photosphere from 0 till $\sim$ 30 days, and at the inner edge of the helium-rich hydrogen envelope after $\sim$ 30 days for models NTLB (solid line) and LB (dotted line)

Note that the light curves of model LB are computed only up to 31.4 days. The reason is that, as the envelope expands after the second peak, the radiative diffusion reduces the internal energy of the expanding matter, and it completely recombines (Figs. 10 and 11). By day $\sim$ 30 the envelope becomes optically thin, and the visual luminosity of model LB abruptly drops in contrast with that of model NTLB (Fig. 13 and 14). Thus neglecting nonthermal processes fails to reproduce the observed bolometric and visual light curves of SN 1993J after the second peak.

In model NTLB the smoothness of the bolometric and visual light curves after the second peak is a direct evidence for dominant nonthermal ionization and excitation. So this stage should be called as a stage of nonthermal ionization and excitation. The evolution of the fraction of ionized hydrogen and once-ionized helium in model NTLB shows that around day 18 the envelope matter stops to recombine and then begins to reionize due to nonthermal processes as opposed to that of model LB (Figs. 10 and 11). As the supernova envelope expands, its ionization balance becomes more and more dominated by nonthermal ionization. The state of the gas deviates more and more from thermodynamic equilibrium. By day 28, the ionization balance of the gas is completely determined by nonthermal processes. Note that at this time the fraction of ionized hydrogen is comparable to that of once-ionized helium in spite of differences in their ionization potentials. It is a characteristic feature of nonthermal ionization. Thus, beginning around day 30 the stage of nonthermal ionization and excitation sets in, which is also confirmed by the emergence of helium lines in the optical spectrum studied below.

4.5. Radioactive ^{56}Ni distribution

During the two last phases discussed above the bolometric light curve evidently depends on the total mass and distribution of radioactive material. The total mass of radioactive ^{56}Ni is mainly constrained by the decline rate of the bolometric luminosity tail and is found to be 0.078 $M_{\odot}$. In turn, the radioactive ^{56}Ni distribution affects the luminosity minimum, the subsequent rise of the luminosity to the second peak, the luminosity maximum, and its date. A good fit to the light curve of SN 1993J can be obtained if the bulk of the radioactive material is confined to layers of the ejected envelope expanding with velocities less than $\sim$ 3800 km s^{-1}. The fact that the emergence of helium lines and the profile of the He I line λ5876Å at day 30 (calculated for model NTLB and discussed below) are consistent with spectral observations of SN 1993J suggests that not only the radial velocity and density profile in the hydrodynamical model, but also the radioactive ^{56}Ni distribution are relevant to those in the ejected envelope of SN 1993J and hence strengthens the above conclusion.

4.6. Comparison to photometric observations

During the first 50 days both the calculated bolometric and visual light curves are in a very good agreement with those observed (Figs. 9 and 13). The calculated effective temperature and B-V colour index agree well with those observed too (Figs. 8 and 15). But the calculated effective temperature and photospheric velocity between day $\sim$ 20 and day $\sim$ 40 and the calculated B-V colour index after day $\sim$ 20 depart from the observations (Figs. 8, 6, and 15). This fact is most likely caused by using the diffusion approximation for the radiative hydrodynamics which results in an overestimate of the temperature gradient in the outer envelope layers (Höflich et al. 1993a).

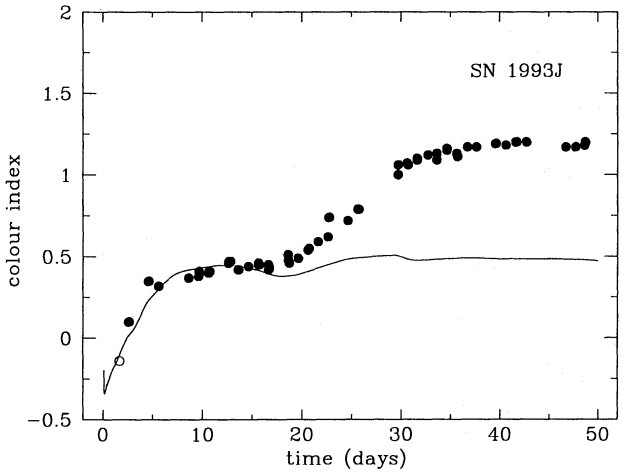

Fig. 15. Comparison of the calculated B-V colour index of model NTLB (solid line) with the observational data of SN 1993J for the first 50 days. Open circle is the CCD observation of Zurek et al. (1993) and solid circles are those of Richmond et al. (1994)

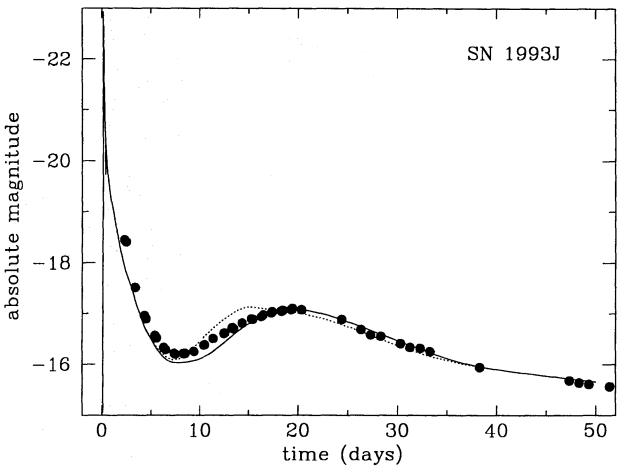

Fig. 17. Comparison of the calculated light curve of models NTLB (solid line) and HESH (dotted line) with the bolometric data for SN 1993J obtained by Lewis et al. (1994)

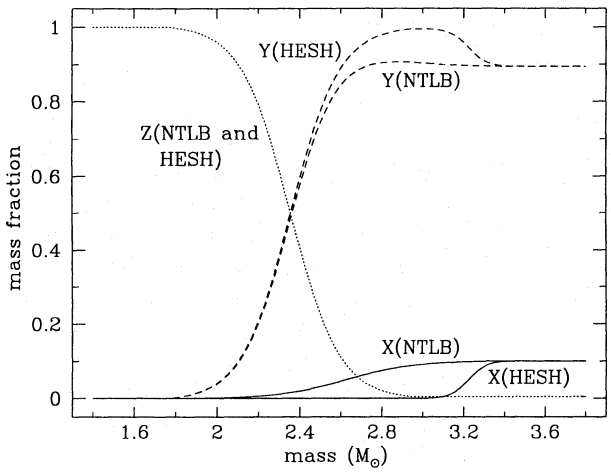

Fig. 16. The mass fraction of hydrogen (X), helium (Y), and heavy elements (Z) in the ejected envelope for models NTLB and HESH. Model HESH has a nearly pure helium mantle between interior mass of $\sim 2.7\ M_\odot$ and $\sim 3.2\ M_\odot$ at level of the helium mass fraction of 0.95. The central core of $1.4\ M_\odot$ is omitted

4.7. Nearly pure helium mantle

The characteristic feature of the chemical composition of model NTLB (Fig. 2) derived from a fit of the observed bolometric and visual light curves is that hydrogen is distributed essentially over the outer part of the ejected envelope and that there is no substantial nearly pure helium mantle. Such a nearly pure helium mantle forms in most of the evolutionary models by the time of explosion including the evolution of massive stars in close binaries (Yamaoka & Nomoto 1991; Woosley et al. 1994). It is therefore reasonable to study an influence of the helium mantle on supernova properties.

To illustrate this influence, we compare model NTLB with a special model HESH differing from it only in the nearly pure helium mantle (Fig. 16). It is evident that at a given content of heavy elements a higher helium abundance leads to a lower opacity of mixture. A decrease in the opacity of the helium mantle of model HESH turns out to result in two unfavourable facts. First, a rise of the bolometric luminosity of model HESH to maximum comes well earlier than those observed and of model NTLB (Fig. 17). Second, between day $\sim$ 12.5 and day $\sim$ 19.4 there is a feature, like a bulge, in the effective temperature whereas the observed effective temperature and that of model NTLB are smooth (Fig. 18). In addition, the helium mantle of model HESH shifts the characteristic maximum of hydrogen number density in the expelled envelope to a significantly higher velocity of $\sim$ 10000 km s^{-1} than that observed in Hα emission at epochs of 0.5 – 1 year after the explosion. Note that the first shortcoming of model HESH may be somewhat improved by shrinking the radioactive material to the more internal layers of the ejected envelope than those in model NTLB, but the rest of them may be removed only by eliminating the nearly pure helium mantle. Thus a nearly pure helium mantle in the ejected envelope is inconsistent with observations of SN 1993J.

5. Helium spectral lines

The stage of nonthermal ionization and excitation, described above and derived from modeling the SN 1993J light curve, should be confirmed observationally. According to Lucy (1991), the presence of strong helium lines in the optical spectra of SNe Ib can be considered as a manifestation of nonthermal excitation. Spectra of SN 1993J began to reveal gradually remarkable lines of helium shortly after day $\sim$ 25 that became prominent by day $\sim$ 30 (Lewis et al. 1994; Richmond et al. 1994; Wheeler & Filippenko 1994). As pointed out above, Swartz et

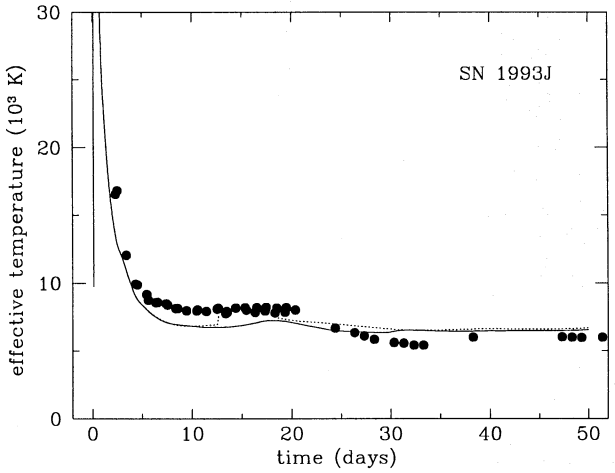

Fig. 18. Time dependence of the effective temperature. The solid and dotted lines represent models NTLB and HESH, respectively. Solid circles give the observational data for SN 1993J obtained by Lewis et al. (1994)

al. (1993) analyzed spectra of SN 1993J at day $\sim$ 40 after the explosion, when strong helium lines had already developed in the optical spectrum and infrared as well. Here we investigate the emergence of helium lines in the optical spectrum and its connection to the stage of nonthermal ionization and excitation. In order to follow the observed transition to strong helium lines, their formation under nonthermal excitation in the frame of our favored hydrodynamical model NTLB is carried out.

5.1. Line formation

In accordance with the supernova hydrodynamical model studied, we suppose that there is a blackbody-emitting photosphere at the corresponding photospheric radius and with the proper effective temperature. The photosphere specifies the external radiation field at any point in the supernova atmosphere extended above it. The density profile in the atmosphere and the kinetic temperature of thermal electrons are also taken from the hydrodynamical model. Solving the equations of statistical equilibrium discussed below at different radii, we can calculate the level populations for the He I atom and find the Sobolev optical depth and the source function for each transition. Once the Sobolev optical depth and the line source function are known, the emergent line flux can be computed by means of the Sobolev method for solving the radiative transfer problem in moving atmospheres (Castor 1970).

5.2. Statistical equilibrium

The adopted model of the He I atom includes the singlet and triplet levels up to 3^1D and 3^3D, respectively. The oscillator strengths for allowed transitions are taken from Wiese et al. (1966). The emission probabilities for the forbidden transitions from the metastable 2^3S and 2^3P states are taken from Drake (1971) and Elton (1967), respectively. The rates of photoexcitation and de-excitation are determined by the dilute photospheric continuum and the local line source functions, with photon trapping treated in the fashion of the Sobolev escape probabilities (Castor 1970). The two-photon decay rates of the metastable 2^1S and 2^3S states are given by Jacobs (1971) and Drake et al. (1969). Fit coefficients for photoionization cross-sections obtained by Koester et al. (1985) are used to calculate photoionization rates and those of spontaneous and stimulated radiative recombinations. The rate coefficients for the electron collisional excitations and de-excitations are computed from effective collision strengths of Berrington & Kingston (1987). The electron collisional ionization and recombination rates are given by the approximate formulae of Mihalas & Stone (1968). The rates of nonthermal excitation of the He I levels are calculated with the excitation fractions taken from Kozma & Fransson (1992). This model of the He I atom is incorporated into the non-LTE ionization balance described above.

5.3. Emergence of helium lines

It is clear that in the supernova hydrodynamical model there are only two opportunities for helium lines to appear in the optical spectrum during the first 50 days (Fig. 14). First, between day $\sim$ 1 and day $\sim$ 3, at the stage of intensive cooling and recombination, helium becomes once-ionized at the photosphere and its lines might be expected to appear in the spectrum. However, the calculations of helium lines do not support these expectations. For example, the calculated profile of He I line λ5876Å is too subtle to be distinct (Fig. 19).

Second, after day $\sim$ 18 the ionization balance becomes more and more dominated by nonthermal ionization as well as the He I level populations by nonthermal excitation (Figs. 11 and 20). Departure coefficients for the 2^1S and 2^3S levels show that He I levels are strongly overpopulated and that these overpopulations are nearly identical for the corresponding levels in the singlet and triplet series. Note that the last fact was found empirically by Harkness et al. (1987) in analyzing He I lines in the spectra of SNe Ib and was confirmed theoretically by Lucy (1991). Nonthermal excitation results in developing strong helium lines in the optical spectrum by day $\sim$ 30 as illustrated by the evolution of the calculated profile of the He I line λ6678Å (Fig. 21).

It is worth to note that, according to Swartz et al. (1993), strong helium lines become visible after (a) the helium-rich hydrogen layer recombined, allowing exposure of the underlying helium mantle; (b) the onset of substantial γ-ray deposition in the helium layer; and (c) the free electron density in the mantle declined sufficiently due to expansion and cooling to eliminate veiling of the helium lines by electron scattering. From the chemical composition of the expelled envelope and the evolution of the fraction of ionized hydrogen and once-ionized helium the conditions described above are evident (Figs. 2, 10, 11, and 21). Hence, an emergence of helium lines in the optical spectrum reproduced in the hydrodynamical model NTLB confirms the conclusions of Swartz et al. (1993).

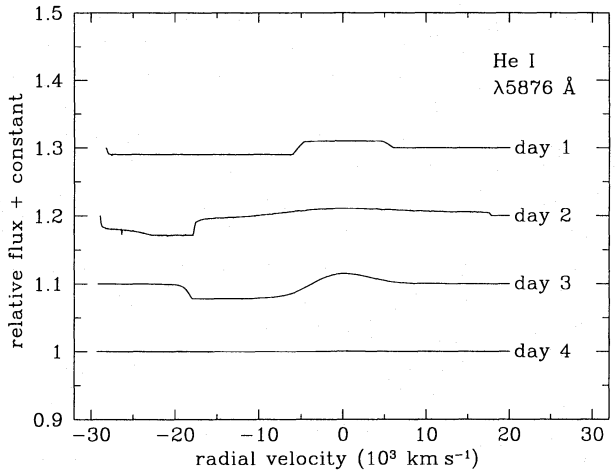

Fig. 19. Evolution of the calculated profile of the He I line λ5876Å for model NTLB. All but the final profile are displayed vertically for clarity

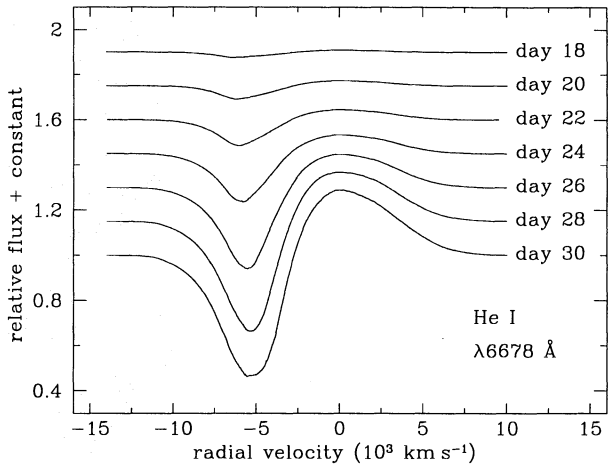

Fig. 21. Evolution of the calculated profile of the He I line λ6678Å for model NTLB. All but the final profile are displayed vertically for clarity

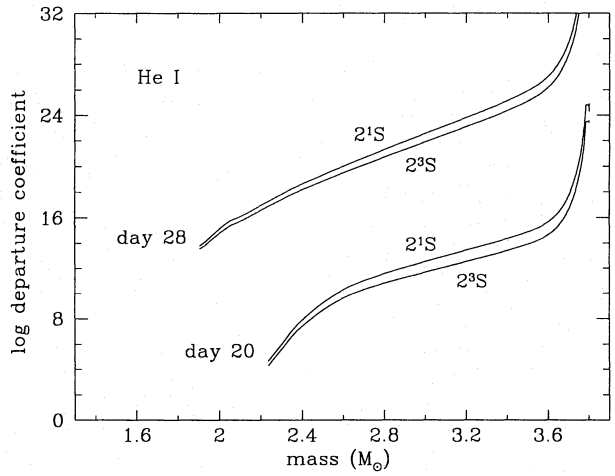

Fig. 20. Evolution of the departure coefficients for the indicated He I levels as a function of mass for model NTLB. Departure coefficient profiles are plotted at the indicated elapsed times

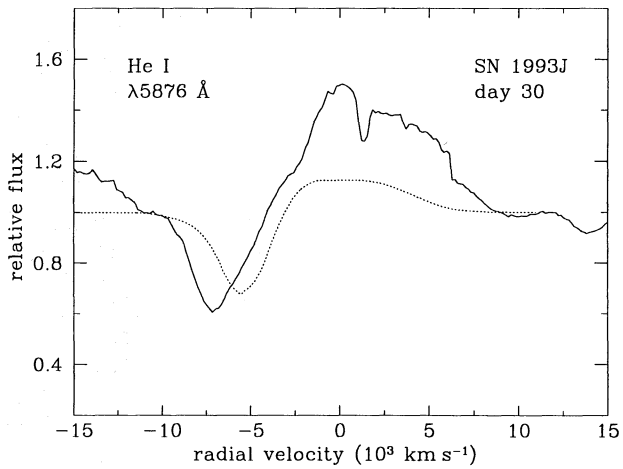

Fig. 22. Comparison of the calculated profile of the He I line λ5876Å at day 30 for model NTLB (dotted line) with that observed on April 28 in SN 1993J by Lewis et al. (1994) (solid line). The latter is shifted by -135 km s^{-1} to place it at the rest wavelengths (Vladilo et al. 1993)

At day 30, when helium lines have become prominent in the optical spectrum, the calculated absorption of the He I line λ5876Å for model NTLB is in a reasonable agreement with that observed on April 28 (Fig. 22). So, the He I excitation picture in expanding atmosphere is relevant to that in the envelope of SN 1993J. Note that the observed blueshift of the absorption minimum of ~ 7100 km s^{-1} is somewhat greater than the calculated blueshift of ~ 5600 km s^{-1}.

It is totally clear that the emergence of helium lines in the calculated spectra is directly connected to the stage of nonthermal ionization and excitation, and is completely consistent to that observed in the optical. Thus, an existence of the stage of nonthermal ionization and excitation is confirmed by the spectral observations of SN 1993J and it begins around day 30 after the explosion.

6. Discussion and conclusions

The aim of this paper is to show that both a smooth tail of the light curve and the emergence of helium lines in the spectrum similar to those observed in SN 1993J can be understood in terms of nonthermal ionization and excitation. The resulting hydrodynamical model succeeds in reproducing the observed features. The bolometric and visual light curves and the spectral evolution of helium lines are consistent with a mass of the ejected envelope of 2.4 $M_\odot$ including a hydrogen mass of 0.12 $M_\odot$, an explosion energy of $1.6 \cdot 10^{51}$ ergs, and a mass of radioactive ^{56}Ni of 0.078 $M_\odot$, the bulk of which is confined to layers ejected with velocities less than ~ 3800 km s^{-1}.

The ejected envelope of 2.4 $M_\odot$ and a neutron star of 1.4 $M_\odot$ correspond to a 3.8 $M_\odot$ progenitor. The helium core of ~ 3 $M_\odot$ in the presupernova model (Fig. 2) presumably stems from a ~ 13 $M_\odot$ main-sequence star (Woosley et al. 1994). So the progenitor must have lost most of its hydrogen-rich envelope prior to the explosion either by stellar winds or by binary mass transfer. Stars of ~ 13 $M_\odot$ are thought to have too low mass loss to lose their hydrogen envelope before core collapse without mass transfer. Modern standard evolution of a single moderately massive star with an initial mass of 15 $M_\odot$ results in a hydrogen-rich star of ~ 12.8 $M_\odot$ at the time of carbon exhaustion in the center (Maeder 1987). On the other hand, in a close binary system, a primary component with an initial mass of 12 $M_\odot$ evolves to a hydrogen-poor star of ~ 3 $M_\odot$ at the end of core helium burning (de Loore & De Greve 1992), while a star with an initial mass of 13 $M_\odot$ evolves to a helium star of ~ 3.7 $M_\odot$ at the end of neon burning (Woosley et al. 1994). Thus, most probably the progenitor has been a member of an interacting binary system. A binary system is known to remain bound after a supernova explosion when the mass ejected in the explosion is less than half of the total mass of the system. In the case of SN 1993J, this implies a companion star more massive than the Sun. Hence, the system is definitely to become a binary system involving a neutron star.

A critical parameter in hydrodynamical models of SN 1993J is the mass of hydrogen and its distribution in the expelled envelope. Shigeyama et al. (1994) showed that the observed light curve of SN 1993J was well reproduced by the explosion of a red supergiant if the mass of its hydrogen-helium envelope had been decreased below ~ 0.9 $M_\odot$ and its underlying helium core had a mass of ~ 4 $M_\odot$. In turn, Woosley et al. (1994) argued that the presupernova had a helium core mass of 4.0 ± 0.5 $M_\odot$ and a hydrogen-helium envelope of 0.20 ± 0.05 $M_\odot$ with a hydrogen mass fraction of ~ 0.5.

In analyzing the spectra of SN 1993J at day ~ 40 after the explosion, Swartz et al. (1993) found that the presence of helium lines was consistent with atmosphere models having parameters similar to those of the hydrodynamical model under study. The mass of the presupernova star at core collapse was ~ 4.0 $M_\odot$ and the mass of the ejected envelope was ~ 2.5 $M_\odot$, of which an outer helium-rich hydrogen layer of ~ 0.4 $M_\odot$ was contaminated with a hydrogen mass fraction of ~ 0.1. In addition, Baron et al. (1994) showed that the ultraviolet and optical spectra of SN 1993J at a phase of ~ 17 days required a high helium mass fraction of ~ 0.8 in the outer layers of the ejected envelope.

Of great importance is the Hα emission line in the late time spectra of SN 1993J at epochs of $0.5 - 1$ year after the explosion. Patat et al. (1994) have analyzed this Hα emission line and have shown that in order for the Hα emission to be reproduced by recombination, the hydrogen mass should be in range of $0.05 - 0.2$ $M_\odot$. So it is clear that there is good, but not convincing, agreement about the hydrogen mass of SN 1993J.

To fit the bolometric and visual light curves of SN 1993J, an outer layer of ~ 1 $M_\odot$ has to be a helium-rich hydrogen shell with a hydrogen mass fraction of ~ 0.1. It is remarkable that in this shell there is no nearly pure helium mantle. Such a distribution of hydrogen has a characteristic maximum at a velocity of ~ 8600 km s^{-1} in the expelled envelope. It is clear that the calculated distribution of hydrogen is well consistent with the late time observations of Hα emission (Patat et al. 1994) and that the above hydrogen mass fraction is very close to those of Swartz et al. (1993) and Baron et al. (1994).

A lack of the nearly pure helium mantle in the ejected envelope of our favored hydrodynamical model conflicts with most of the evolutionary models including the evolution of massive stars in close binaries (Yamaoka & Nomoto 1991; Woosley et al. 1994). If the chemical composition of the ejected envelope described above is the right configuration, a nature of the evolution of massive stars and, perhaps, the subsequent mixing need some reconsideration. Note that Woosley et al. (1994) have already used a moderate amount of artificial mixing after explosive nucleosynthesis in order to improve a fit to observations of SN 1993J.

The second issue deals with the opportunity to set up constraints on the amount of mixing of ^{56}Ni in analyzing the photometric data of SN 1993J, because the total mass of radioactive ^{56}Ni is mainly determined by the decline rate of the bolometric luminosity tail. In order to reproduce the observed bolometric light curve of SN 1993J, Shigeyama et al. (1994) assumed radioactive ^{56}Ni to be mixed throughout the helium core, the outer edge of which expanded with a velocity of ~ 7000 km s^{-1}. Using similar arguments, Woosley et al. (1994) concluded that a moderate amount of outward mixing of ^{56}Ni took place in SN 1993J, with a characteristic velocity of the ^{56}Ni-rich layers being of ~ 5600 km s^{-1}. In the present model of SN 1993J the bulk of the radioactive material is confined to layers of the ejected envelope expanding with velocities less than ~ 3800 km s^{-1}. It is thus not clear how much mixing is necessary to satisfy the photometric observations of SN 1993J. However, it should be emphasized that in our model the amount of mixing of ^{56}Ni in the ejecta of SN 1993J obtained from fitting the light curves is completely consistent with an emergence of helium lines in the optical.

A characteristic transformation of SN 1993J as well as of SN 1987K from spectra of SNe II to those of SNe Ib suggests that SNe IIb are related to SNe Ib (Filippenko 1988; Filippenko et al. 1993). To check this important relation it is worth while to compare the quantity of oxygen ejected by these supernovae, a fundamental parameter for setting the evolutionary status of the presupernova star. The oxygen mass of Type Ib SN 1985F and SN 1984L appeared to be ~ 1 $M_\odot$ (Fransson & Chevalier 1989; Schlegel & Kirshner 1989; Tutukov & Chugai 1992) and the oxygen-rich layers expanded with a characteristic velocity of ~ 4200 km s^{-1} and ~ 4700 km s^{-1}, respectively (Schlegel & Kirshner 1989). Our model of SN 1993J implies that the mass of oxygen is at most ~ 1 $M_\odot$ and that those layers expand with velocities as high as ~ 4000 km s^{-1}. Thus there is a good match between this model of SN 1993J and SNe Ib. Another important parameter is the amount of mixing of ^{56}Ni in the supernova ejecta. In our model of SN 1993J the layers of the ejected envelope contaminated with the radioactive material expand with velocities less than ~ 3800 km s^{-1}. This is consistent with an

expansion velocity of 2500 ± 1000 km s^{-1} derived from infrared observations of iron emission lines at 1.6 μm in the Type Ib SN 1983N (Graham et al. 1986).

Of particular interest is the stage of nonthermal ionization and excitation and its existence in other supernovae. It is clear that the presence of strong helium lines in spectra of SN 1993J and SNe Ib, and the striking similarity of the bolometric light curve of SN 1993J near the second maximum to that of the Type Ib SN 1983N pointed out by Nomoto et al. (1993) result from the close physical conditions in their expanding envelopes. Thus, it is extremely reasonable to expect the existence of a stage of nonthermal ionization and excitation in SNe Ib, too. Based on our model of SN 1993J, we also predict that the light curves of SNe Ib should be subject to nonthermal ionization and excitation at earlier times than even that of SN 1993J, because of the presence of rather strong helium lines in their spectra before maximum light (Wheeler & Swartz 1991).

The hydrodynamical model of SN 1993J discussed here implies that most likely it is a core collapse supernova rather than a thermonuclear explosion. The modern theory of core collapse and bounce of $8 - 15$ $M_\odot$ main-sequence stars remains controversial and no satisfactory detailed mechanism has been proposed so far (Woosley & Weaver 1986; Hillebrandt 1991; Janka & Müller 1994; Burrows 1994). For this reason SN 1993J and the well-studied Type II-P SN 1987A, which definitely underwent core collapse, should be compared. First, the explosion energy of $1.6 \cdot 10^{51}$ ergs is nearly equal to that of SN 1987A (Woosley 1988; Shigeyama & Nomoto 1990; Utrobin 1993). Second, the mass of radioactive ^{56}Ni of ~ 0.078 $M_\odot$ is very close to that of SN 1987A (Suntzeff et al. 1991). Thus, there are strong arguments in favor of a fundamental similarity between the explosions of SNe IIb and SNe II-P.

Wheeler & Levreault (1985) defining the new subclass of SNe Ib concluded that SNe Ib, similar to SNe II, came from core collapse in moderately massive stars which, in contrast to SNe II, lost their hydrogen envelopes due to strong stellar winds or binary mass transfer and which had masses as low as 3 $M_\odot$ at the time of explosion. According to Ensman & Woosley (1991), the majority of SNe Ib result from hydrogen-stripped stars of $4 - 7$ $M_\odot$ undergoing mass transfer in interacting binary systems. Shigeyama et al. (1990) argued that SNe Ib and typical SNe II-P originate from a similar mass range on the main sequence and that the progenitors of SNe Ib in contrast to those of SNe II are most probably helium stars of $3 - 4$ $M_\odot$ which are produced by moderately massive stars in binary systems. The results of our investigation of SN 1993J are consistent with the above hypothesis for the origin of SNe Ib and hence strengthen it. Moreover, from the above discussion a physical similarity of SNe Ib, SNe IIb, and SNe II-P becomes evident now.

Acknowledgements. The author thanks N. Chugai and E. Müller for helpful discussions, P. Höflich for providing him with tables for the Rosseland mean expansion opacity and the enhancement factor, and F. Patat for providing him with a manuscript prior to publication. The author wishes to thank E. Müller for a careful and critical reading of the manuscript and is grateful to him for his hospitality at the Max-Planck-Institut für Astrophysik where this paper was written. The author is also grateful to the referee, J. Craig Wheeler, for a number of critical comments and suggestions which helped improving the manuscript. The calculations were carried out on the CRAY Y-MP4 of the Rechenzentrum Garching. The spectral data used in this paper are obtained by the 2.5-m Isaac Newton Telescope which is operated on the island of La Palma by the Royal Greenwich Observatory in the Spanish Observatorio del Roque de los Muchachos of the Instituto de Astrofisica de Canarias. This work has been supported in part by the Russian Foundation for Fundamental Research (94-02-17114) and the International Science Foundation (M9E000).

References

Aldrovandi S.M.V., Péquignot D., 1973, A&A 25, 137
Allen C.W., 1973, Astrophysical quantities. The Athlone Press, London
Ambwani K., Sutherland P., 1988, ApJ 325, 820
Baron E., Hauschildt P.H., Branch D., 1994, ApJ 426, 334
Bartunov O.S., Blinnikov S.I., Pavlyuk N.N., Tsvetkov D.Yu., 1994, A&A 281, L53
Berrington K.A., Kingston A.E., 1987, J. Phys. B 20, 6631
Burrows A., 1994, Proc. The 17th Texas Symposium on Relativistic Astrophysics (submitted)
Castor J.I., 1970, MNRAS 149, 111
Colgate S.A., Petschek A.G., Kriese J.T., 1980, ApJ 237, L81
de Loore C., De Greve J.P., 1992, A&AS 94, 453
Doughty N.A., Fraser P.A., 1966, MNRAS 132, 267
Drake G.W.F., 1971, Phys. Rev. A 3, 908
Drake G.W.F., Victor G.A., Dalgarno A., 1969, Phys. Rev. 180, 25
Elton R.C., 1967, ApJ 148, 573
Ensman L., Woosley S.E., 1991. In: Woosley S.E. (ed.) The tenth Santa Cruz Workshop, Supernovae. Springer-Verlag, New York, p. 556
Filippenko A.V., 1988, AJ 96, 1941
Filippenko A.V., Matheson T., Ho L.C., 1993, ApJ 415, L103
Fransson C., Chevalier R.A., 1989, ApJ 343, 323
Freedman W.L., Hughes S.M., Madore B.F., et al. , 1994, ApJ 427, 628
Garcia F., 1993, IAU Circs. 5731, 5733
Graham J.R., Meikle W.P.S., Allen D.A., Longmore A.J., Williams P.M., 1986, MNRAS 218, 93
Harkness R.P., Wheeler J.C., Margon B., et al. , 1987, ApJ 317, 355
Hillebrandt W., 1991. In: Danziger I.J., Kjär K. (eds.) Proc. ESO/EIPC Workshop, Supernova 1987A and other supernovae. ESO, Garching, p. 55
Höflich P., Müller E., Khokhlov A., 1993a, A&A 268, 570
Höflich P., Langer N., Duschinger M., 1993b, A&A 275, L29
Jacobs V., 1971, Phys. Rev. A 4, 939
Janka H.-T., Müller E., 1994, Physics Reports (in press)
Karp A.H., Lasher G., Chan K.L., Salpeter E.E., 1977, ApJ 214, 161
Kato T., 1993, IAU Circs. 5747, 5750, 5755
Koester D., Vauclair G., Dolez N., et al. , 1985, A&A 149, 423
Kozma C., Fransson C., 1992, ApJ 390, 602
Levermore C.D., Pomraning G.C., 1981, ApJ 248, 321
Lewis J.R., Walton N.A., Meikle W.P.S., et al. , 1994, MNRAS 266, L27
Lucy L.B., 1991, ApJ 383, 308
Maeder A., 1987, A&A 173, 247
Mihalas D., Stone M.E., 1968, ApJ 151, 293
Neely A., 1993, IAU Circ. 5740

Nomoto K., Suzuki T., Shigeyama T., et al. , 1993, Nat 364, 507 1994, ApJ 420, 341
Osterbrock D.E., 1989, Astrophysics of gaseous nebulae and active galactic nuclei. University Science Books, Mill Valley, California
Patat F., Chugai N., Mazzali P.A., 1994, A&A (submitted)
Podsiadlowski Ph., Hsu J.J.L., Joss P.C., Ross R.R., 1993, Nat 364, 509
Pujol P., 1993, IAU Circ. 5731
Richmond M.W., Treffers R.R., Filippenko A.V., et al. , 1994, AJ 107, 1022
Rodriguez D., 1993, IAU Circ. 5731
Schlegel E.M., Kirshner R.P., 1989, AJ 98, 577
Shigeyama T., Nomoto K., 1990, ApJ 360, 242
Shigeyama T., Nomoto K., Tsujimoto T., Hashimoto M., 1990, ApJ 361, L23
Shigeyama T., Suzuki T., Kumagai S., et al. , 1994, ApJ 420, 341
Shull J.M., Van Steenberg M., 1982, ApJS 48, 95
Suntzeff N.B., Phillips M.M., Depoy D.L., Elias J.H., Walker A.R., 1991, AJ 102, 1118
Sutherland P.G., Wheeler J.C., 1984, ApJ 280, 282
Swartz D.A., Clocchiatti A., Benjamin R., Lester D.F., Wheeler J.C., 1993, Nat 365, 232
Tutukov A.V., Chugai N.N., 1992, Sov. Astr. Lett. 18, 242
Utrobin V.P., 1993, A&A 270, 249
Utrobin V.P., 1994a, A&A 281, L89
Utrobin V.P., 1994b, Proc. The 17th Texas Symposium on Relativistic Astrophysics (submitted)
Vladilo G., Centurión M., de Boer K.S., et al. , 1993, A&A 280, L11
Wiese W.L., Smith M.W., Glennon B.M, 1966, Atomic Transition Probabilities. Volume I. Hydrogen Through Neon. NSRDS-NBS 4
Wheeler J.C., Filippenko A.V., 1994. In: McCray R.A., Wang Z., Li Z. (eds.) Proc. IAU Coll. 145, Supernovae and supernova remnants. Cambridge Univ. Press, Cambridge (in press)
Wheeler J.C., Levreault R., 1985, ApJ 294, L17
Wheeler J.C., Swartz D.A., 1991, PASP 103, 787
Wheeler J.C., Barker E., Benjamin R., et al. , 1993, ApJ 417, L71
Woosley S.E., 1988, ApJ 330, 218
Woosley S.E., Weaver T.A., 1986, ARA&A 24, 205
Woosley S.E., Eastman R.G., Weaver T.A., Pinto P.A., 1994, ApJ 429, 300
Yamaoka H., Nomoto K., 1991. In: Danziger I.J., Kjär K. (eds.) Proc. ESO/EIPC Workshop, Supernova 1987A and other supernovae. ESO, Garching, p. 193
Zurek D.R., Robb R.M., Balam D.D., 1993, IAU Circ. 5761

This article was processed by the author using Springer-Verlag LaTeX A&A style file version 3.